Homogeneous, Competitive Fluorescence Quenching Immunoassay Based on Gold Nanoparticle/Polyelectrolyte Coated Latex Particles

Noritaka Kato[†] **and Frank Caruso***

Centre for Nanoscience and Nanotechnology, Department of Chemical and Biomolecular Engineering, The University of Melbourne, Victoria 3010, Australia

Received: May 25, 2005; In Final Form: August 4, 2005

This study reports a homogeneous and competitive fluorescence quenching immunoassay based on gold nanoparticle/polyelectrolyte (Au_{NP}/PE) coated latex particles prepared by the layer-by-layer (LbL) technique. First, the resonant energy transfer from a layer of fluorescent PEs to Au_{NP} in LbL assembled films on planar substrates was investigated. The quenching efficiency (QE) for the planar films depended on the cube of the distance between the two layers. A QE of 50% was achieved at a distance of ca. 15 nm, indicating that the Au_{NP}/PE system is suitable for detecting binding/release events for antibodies. A homogeneous, competitive binding immunoassay for biotin was designed based on Au_{NP}/PE-coated polystyrene particles of 488 nm diameter as quenching agents for a fluorescein isothiocyanate labeled anti-biotin immunoglobulin (FITC-anti-biotin IgG). Biotin molecules were localized on the Au_{NP}/PE-coated latexes by depositing a layer of biotinylated poly(allylamine hydrochloride) (B-PAH), and FITC-anti-biotin IgGs were subsequently bound to the particles through interaction with the biotin on B-PAH. Transmission electron microscopy and quartz crystal microgravimetry confirmed the multilayer formation on latex particles and planar gold surfaces, respectively. The biotin-functionalized Au_{NP}/PE-coated latexes terminated by FITC-anti-biotin IgG exhibited a dynamic sensing range of 1−50 nmol. These results indicate that Au_{NP}/PE-coated latexes can be readily used as dynamic range tunable sensors.

Introduction

There have been a number of developments in fluorescence immunoassays (FIAs), and numerous fluorophores and methods have been proposed.[1−3] A promising approach is based on fluorescence quenching immunoassays (FQIAs), where extensive studies on fluorescence quenching by metals have been conducted.[4−12] When a fluorophore is close to a metal surface, energy transfer (ET) from the fluorophore to the metal occurs, resulting in fluorescence quenching. This allows monitoring of receptor/ligand binding and release events through changes in the fluorescence intensity or lifetime of the fluorophore. Metal films deposited on planar substrates and dispersed metal (gold and silver) nanoparticles have been applied as quenchers in FQIAs.[4−12] Surface plasmon (SP) modes have been utilized to effect resonant ET or excitation enhancement, resulting in a higher degree of quenching or emission, reflecting binding and unbinding states of analytes to sensors. Despite such studies, metal nanoparticles supported on colloidal submicron-sized particles have not been applied in FQIAs. Compared with metal-coated planar films or nanoparticles, the application of colloidally stable nanoparticle-coated submicron-sized colloids in FQIAs offers the combined advantage of both methods: the ability to tailor the surface functionality to the same level as for planar substrates, high surface area for analyte binding/release, and ease of handling, as the particles can be readily collected through filtration and/or centrifugation, with the potential for reuse. Further, the surface area of the colloidal dispersion can be easily altered by changing the particle concentration, allowing tuning of the dynamic sensing range.

Recently, we showed that gold nanoparticle (Au_{NP}) coated particles with tailored optical properties and nanoparticle loadings could be formed by the layer-by-layer (LbL) technique.[13−18] The particles were prepared by the sequential deposition of oppositely charged polyelectrolytes (PEs) onto colloidal particles, followed by adsorption of ligand-stabilized gold nanoparticles into the PE multilayer films. We applied such particles in photonic crystal studies to modulate the optical properties of colloidal crystals,[13−15] and as optically addressable capsules, which can release (bio)macromolecules upon irradiation with near-infrared light.[16,17] In this study, we design and tailor Au_{NP}/PE-coated latex particles (Au_{NP}/PE latexes) for use as quenching agents in FQIAs. The Au_{NP}/PE latexes were prepared by depositing Au_{NP} on submicron-sized latex spheres precoated with PE multilayers.[13,18] The SP band of the Au_{NP} on the latexes is utilized for the resonant quenching of fluorophores coupled to antibodies, which are attached to the surface of the particles (see Figure 1). When bound on the surface of the Au_{NP}/PE latexes, the fluorescence from the antibodies is quenched due to ET (Figure 1a). After injection of the analytes in the suspension (Figure 1b), the antibodies are competitively released from the Au_{NP}/PE latexes into solution and became fluorescent (Figure 1c), resulting in a homogeneous and competitive binding immunoassay.

We demonstrate a FQIA based on the Au_{NP}/PE latexes by using biotin molecules as analytes, and fluorescein isothiocyanate (FITC) conjugated anti-biotin immunoglobulin (FITC-anti-biotin IgG) as fluorophores (Figure 1).[10] Before preparation of the functionalized latexes, we investigated the quenching efficiency between Au_{NP} and FITC layers to examine the

* Corresponding author. E-mail: fcaruso@unimelb.edu.au.
[†] Present address: Department of Physics, Waseda University, Tokyo 169-8555, Japan.

10.1021/jp052748f CCC: $30.25
Published on Web 10/01/2005

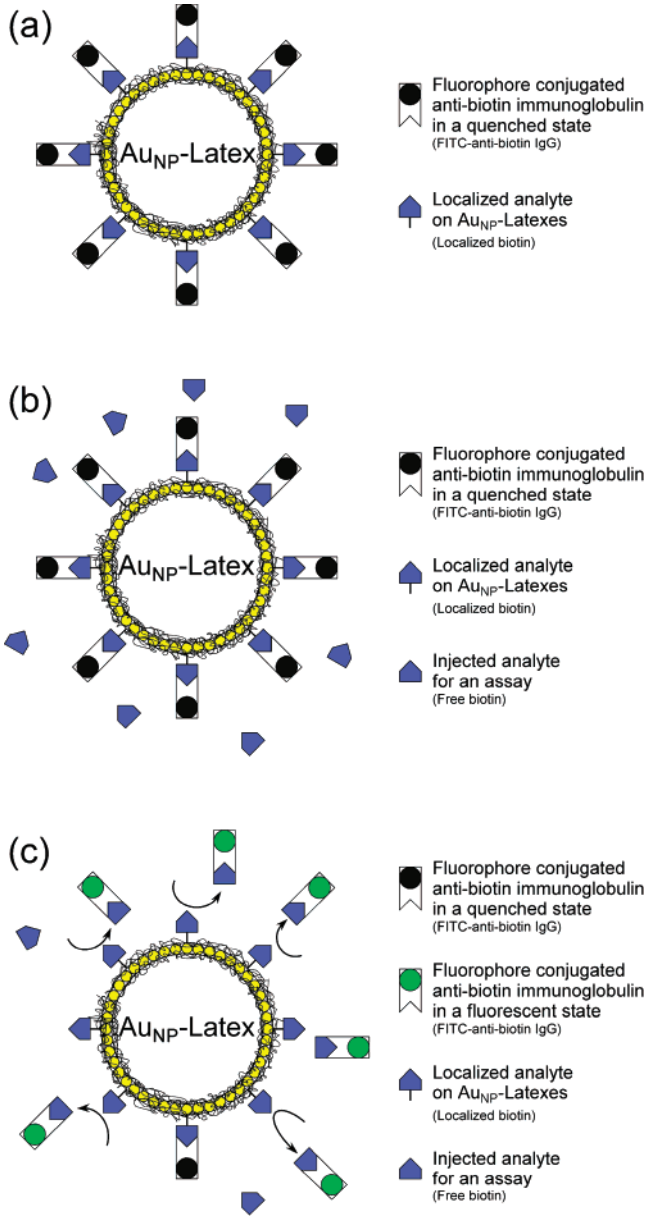

Figure 1. Schematic illustration of competitive FQIA using a suspension of Au_{NP}/PE-coated latexes. (a) Fluorophore-labeled antibodies are quenched before injection of analyte (biotin). (b) Injection of analyte. (c) Fluorophore-labeled antibodies fluoresce after being competitively released by biotin.

properties of resonant ET. This was studied in planar films by changing the amount of Au_{NP} in the layer and the distance between the Au_{NP} and FITC layers. For biotin localization on the Au_{NP}/PE latexes, biotinylated poly(allylamine hydrochloride) (B-PAH) was prepared, and the binding specificity of the B-PAH was confirmed by constructing avidin/B-PAH multilayers on planar supports. The fluorescence intensity of the latex dispersions as a function of analyte concentration was monitored to evaluate the dynamic sensing range for biotin.

Experimental Section

Materials. Poly(sodium 4-styrenesulfonate) (PSS) (M_w = 70 000), poly(ethylene imine) (PEI) (M_w = 25 000), PAH (M_w = 15 000 and 70 000), FITC, dimethyl sulfoxide (DMSO), 4-(dimethylamino)pyridine (DMAP), gold tetrachloride ($HAuCl_4$), sodium borohydride ($NaBH_4$), toluene, 20 wt % aqueous solution of poly(allylamine) (PA) (M_w = 17 000), biotinamidohexanoic acid 3-sulfo-*N*-hydroxysuccinimide ester sodium salt (biotin-ANHS), 4-(2-hydroxyethyl)piperazine-1-ethanesulfonic acid (HEPES), bovine serum albumin (BSA), 2-(4′-hydroxyazobenzene)benzoic acid (HABA), lyophilized powder of avidin, and FITC-conjugated avidin (FITC-avidin) from egg white were purchased from Sigma-Aldrich. Tetraoctylammonium bromide (TOAB), hydrochloric acid (HCl), sodium chloride (NaCl), and sodium hydroxide (NaOH) were from Fluka. Biotin and the FITC-conjugated goat polyclonal anti-biotin immunoglobulin (FITC-anti-biotin IgG) (1 mg mL^{-1} aqueous solution) used for the competitive FQIA were purchased from Sigma-Aldrich. An aqueous HEPES solution (0.01 M, 0.1 M NaCl, pH 7.3 ± 0.1) was used as buffer. For the anti-biotin antibody, the HEPES buffer containing 1 wt % BSA was used to reduce the nonspecific binding. Before use, the buffers were filtered (Minisart, 200 nm pore size, Sartorius). Polystyrene (PS) latexes with a diameter of 488 nm and sulfonated surfaces were purchased from Microparticles GmbH (Berlin, Germany).

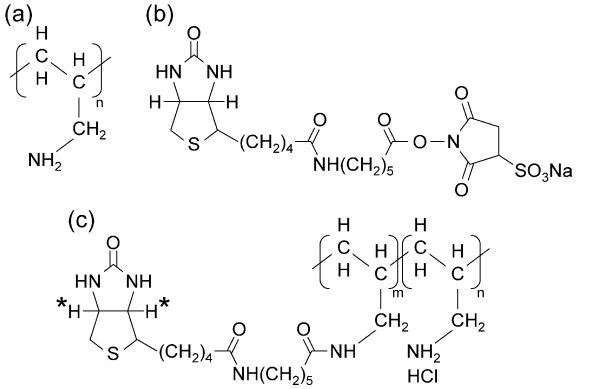

Figure 2. Molecular structures of materials used for biotinylation of PAH. (a) PA, (b) biotin-ANHS, and (c) B-PAH.

Synthesis of Au_{NP} Dispersion. An aqueous suspension of Au_{NP} with an average diameter of ca. 6 nm was prepared, as reported previously.[19] A 30 mL volume of aqueous $HAuCl_4$ (10 mg mL^{-1}) and 80 mL of TOAB in toluene (25 mM) were mixed to transfer the gold salt to the toluene phase. The toluene phase was washed with water until the pH of the separated water became neutral; then 10 mL of aqueous $NaBH_4$ (30 mg mL^{-1}) was slowly added to the separated toluene with stirring. This toluene/aqueous solution was then incubated overnight without stirring, and Au_{NP} were formed in the toluene phase. The toluene phase was again washed with water until the pH of the separated water became neutral. The Au_{NP} were then transferred from toluene to an aqueous DMAP solution by adding 0.1 M DMAP, resulting in a DMAP-stabilized Au_{NP} dispersion, with a SP peak at approximately 518 nm.

Polymer Labeling. FITC-labeled PAH (FITC-PAH) was prepared by a method based on a protein labeling.[20,21] A 0.42 mL volume of FITC in DMSO (10 mg mL^{-1}) was added to 25 mL of aqueous PAH (M_w = 15 000) (4 mg mL^{-1}, pH adjusted to 9.0 by 1 M aqueous NaOH) and gently stirred overnight. The resulting FITC-PAH was then purified by a Slide-A-Lyzer dialysis cassette (3500 MWCO, 3−12 mL capacity, PIERCE). The dialysis was carried out in darkness against pure water for 48 h, renewing the water four times. The degree of the labeling was ca. 1% PAH monomer.[21]

B-PAH was obtained by following a procedure based on reported methods.[22,23] The molecular structures of the materials used are given in Figure 2. A 50 mg sample of 20 wt % aqueous PA and 4 mg of biotin-ANHS were added to 8.5 mL and 1.5 mL of 0.2 M bicarbonate buffer (pH 8.3), respectively. The

solutions were mixed together and stirred overnight to achieve randomly labeled PA with biotin. The stirred solution was then injected into the dialysis cassette (3500 MWCO, 3−12 mL capacity, PIERCE) and dialyzed against water for 96 h. Water for the dialysis was renewed on a 24 h cycle. Pure water was used for the first cycle. For the remaining cycles, water of pH 4, prepared by adding aqueous HCl, was used to convert the amine groups to ammonium groups for improved solubility. After the solution was removed from the dialysis cassette, it was filtered (Minisart, 200 nm pore size, Sartorius) to remove the aggregated PEs, resulting in ca. 50% yield. To evaluate the degree of the labeling, the solvent of the obtained B-PAH solution was exchanged into heavy water and analyzed by nuclear magnetic resonance (NMR). Using the integrated values of two peaks at 4.4 and 4.2 ppm in the proton NMR spectrum, which originate from the two protons of biotin (see the marked protons in Figure 2c),[24,25] the labeling was calculated to be ca. 4% of the monomer units in the polymer.

LbL Coating of Planar Supports and Microspheres. The procedure and conditions used for preparing LbL films are as follows. The polyanion adsorption solution was PSS (1 mg mL^{-1} with 0.5 M NaCl), and the polycation solutions were PEI or PAH (M_w = 70 000) (1 mg mL^{-1} with 0.5 M NaCl). Quartz or glass slides were used as negatively charged substrates after RCA cleaning.[26] The layers were deposited by (i) dipping the glass substrates in the adsorption solution and incubating for a given time, (ii) removing the coated substrate from the adsorption solution and rinsing with a washing solution (e.g., water), and (iii) drying the coated substrate using compressed air. The adsorption time depended on the sample (typically 10 min). In the case where drying after layer deposition was not desired, step iii was omitted. Repetition of these steps, alternating the polycation and polyanion adsorption solutions, resulted in the buildup of PE multilayer thin films. The same adsorption solutions used for the planar substrates were employed for the microspheres (PS latexes). A 25 μL volume of a 1 wt % aqueous suspension of the PS latexes was transferred to a 2 mL centrifuge tube (Eppendorf) and washed with 1.5 mL of pure water three times by centrifugation/water wash cycles. The polycation was then deposited as the first layer because of the negatively charged surface of the PS latexes. For each layer, the following steps were performed: (i) centrifuge (10000*g* for 12 min) the suspension and remove the supernatant; (ii) disperse the sediment using brief sonication (<1 min); (iii) add 1.5 mL of the adsorption solution and incubate for 20 min with agitation; (iv) centrifuge (10000*g* for 12 min) the suspension and remove the supernatant; (v) disperse the sediment with brief sonication; (vi) add 1.5 mL of pure water. The suspension was then cleaned from excess PE through two repeated centrifugation/washing cycles. Repeating these steps with adsorption solutions of the desired oppositely charged PE resulted in LbL films on the PS latexes.

For the FQIAs, the biotin−Au_{NP}/PE latexes terminated with FITC-anti-biotin IgG (PS latex/$(PAH/PSS)_3$/Au_{NP}/$(PEI/PSS)_2$/B-PAH/FITC-anti-biotin IgG) were prepared as follows. Briefly, three PAH/PSS bilayers were coated on the bare PS latexes, followed by Au_{NP} deposition from a DMAP−Au_{NP} suspension for 12 h. Three centrifugation/water washing cycles were performed.[13] Two PEI/PSS bilayers were then deposited, followed by a B-PAH layer (ca. 0.5 mg mL^{-1} solution, no added salt). An adsorption time of 20 min was used for all PE layers, and water was used for the washing steps, which were conducted in triplicate after deposition of each PE layer. FITC-anti-biotin IgG (0.25 mg mL^{-1} in HEPES and containing 1 wt % BSA) was then adsorbed for 12 h. The coated latexes were then washed three times with HEPES buffer (BSA free), and finally dispersed in 1 mL of HEPES buffer.

HABA Assay. A HABA assay was applied to determine the amount of active biotin in the solution.[27] Upon binding to a biotin binding site of avidin, HABA changes its color from yellow to red due to intramolecular charge transfer.[28] When active biotins are in an avidin−HABA complex solution, HABA bound to avidin is replaced by biotin because of the higher affinity of biotin, and the released HABA restores the yellow color. Thus, the amount of active biotin in the solution can be determined through monitoring the color change of HABA. A 10 mM HABA solution was made up in 10 mM aqueous NaOH. A 0.6 mL volume of this HABA solution and 10 mg of avidin were added to 19.4 mL of HEPES buffer, resulting in a solution of the avidin−HABA complex for the HABA assay.

Quartz Crystal Microbalance (QCM) Measurements. QCM devices (HC-49/U, Kyushu Dentsu Co., Ltd.), consisting of AT-cut quartz crystals with a resonant frequency of 9 MHz and gold electrodes of 4.5 mm diameter (on both sides of the quartz) were used to determine the thickness of the coatings. The resonant frequency of the QCM was measured by a frequency counter (HP 53131A) and a home-built oscillator. The surface of the gold electrode on the QCM was cleaned with Piranha solution, and PEI was then coated as a first layer. (***Caution!*** *Piranha solution is highly corrosive. Extreme care should be taken when handling Piranha solution, and only small quantities should be prepared.*) The QCM electrodes were dried with a gentle stream of compressed air after each coating and the frequency change was recorded. The resonant frequency differences between the uncoated and coated QCMs were used to calculate the film thickness by applying the Sauerbrey equation.[29] Using the values of the shear modulus of quartz (2.95×10^{13} g m^{-1} s^{-2}), the density of quartz (2.65×10^6 g m^{-3}), and the initial resonant frequency (9 MHz), the relationship between the total mass difference, Δm (g), and the resonant frequency difference, Δf (Hz), is given as

$$\Delta m = -5.46 \times 10^{-5} A \Delta f \qquad (1)$$

where A (m^2) is the electrode area on one side of the quartz crystal. Using the density of the material ρ_m (g m^{-3}) adsorbed on the QCM, the effective area of the electrode A_{eff} (m^2) on one side of the QCM, and eq 1, the thickness difference, Δd (m), is calculated from Δf according to the equation

$$\Delta d = \frac{\Delta m}{2 A_{eff} \rho_m} = -2.02 \times 10^{-5} \frac{\Delta f}{\rho_m} \qquad (2)$$

Here, A/A_{eff} was empirically assumed as 1/1.35, which is attributed to the surface roughness of the electrode.[26,30,31] A ρ_m of 19.3×10^6 g m^{-3} was used for gold, and 1.2×10^6 g m^{-3} was assumed for the PEs.[30,31]

Spectral Measurements. Absorption spectra of the films and extinction spectra of the suspensions were measured with a Cary 4E double-beam spectrophotometer (Varian) and an 8453 UV−visible spectrophotometer (Agilent Technologies), respectively. Fluorescence spectra were recorded on a Cary Eclipse fluorescence spectrophotometer (Varian) or a SPEX Fluorolog-Tau2 spectrofluorometer (Jobin Yvon), using a detection angle of 90° from the direction of the excitation beam. For the FQIAs, the latter fluorometer was used. The suspension was placed in a disposable cuvette, and stirred during the measurements at 20 °C. The excitation wavelength was 450 nm and the scan range was 480−640 nm in 3 nm steps, integrating at 1 s per point. A

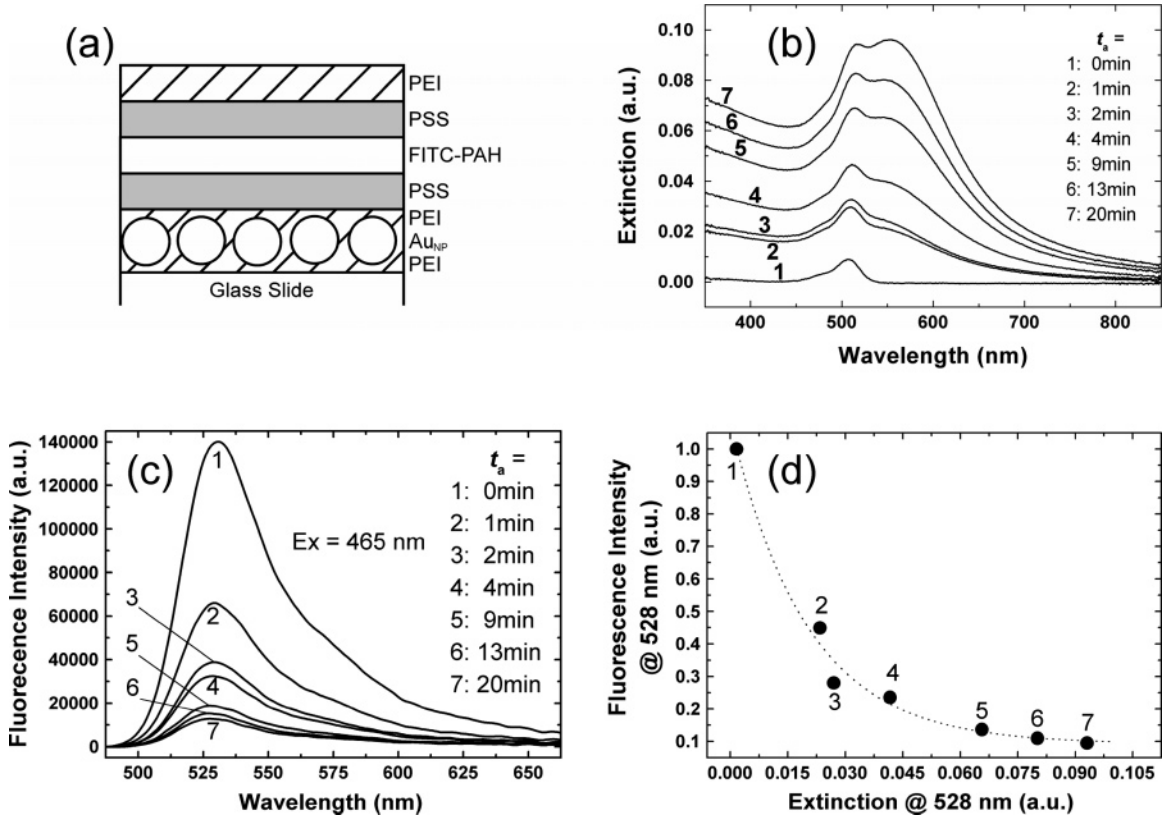

Figure 3. (a) Schematic of the cross section of the LbL film PEI/Au_{NP}/PEI/PSS/FITC-PAH/PSS/PEI deposited on glass. (b) Extinction spectra of the samples incubated in the Au_{NP} dispersion for 0 (line 1), 1 (line 2), 2 (line 3), 4 (line 4), 9 (line 5), 13 (line 6), and 20 min (line 7). (c) Fluorescence spectra of the same samples used in (b). The excitation wavelength was 465 nm. (d) Normalized peak intensity at 528 nm of the spectra in (c) plotted against the extinction observed at 528 nm in (b). Error bars of the fluorescence intensities are within the data points. The dashed curve is drawn to guide the eye.

10 min incubation after each titration of the analyte (biotin) solution was carried out before each measurement to ensure a saturated response.

For investigating the ET properties, the LbL films containing Au_{NP} and FITC-PAH layers were assembled on quartz substrates. Although the FITC-PAH adsorption time was fixed for all samples, the absorbance varied by about 10%. To correct for this, the fluorescence intensities were divided by the amount of FITC adsorbed.

Microscopy. The morphology of the coated latexes was observed using a transmission electron microscope (TEM) (Philips CM 120 BioTWIN) operated at 120 kV. Samples were prepared by depositing a diluted suspension on pioloform-coated copper grids. The concentration of latexes in the suspension was determined with a hemocytometer; that is, the particles in a counting chamber were counted under an optical microscope.

FQIA Experiments. The as-prepared suspension of biotin−Au_{NP}/PE latexes terminated with FITC-anti-biotin IgG were diluted 8-fold with the HEPES buffer, and 2 mL was removed for the assay. Biotin, 0.8 mM in the HEPES buffer, was titrated against this 2 mL suspension. The equilibration time before measuring the fluorescence spectra was 10 min.

Results and Discussion

Planar Films. *(a) Fluorescence Quenching of FITC by Au_{NP}.* To probe the quenching behavior of FITC by the Au_{NP} in the PE layers, two series of experiments were performed on LbL films coated on glass slides. In the first series (I), we examined the quenching dependence on the *amount of Au_{NP}* with a fixed distance between the Au_{NP} and FITC-PAH layers. The second set of experiments (II) involved measuring the quenching dependence on the *distance* between the Au_{NP} and FITC-PAH layers with a fixed Au_{NP} loading.

The sample structure for experiment I is shown in Figure 3a. On both sides of the glass slide, PEI was coated as the first layer; Au_{NP} were then adsorbed, followed by consecutive layers of PEI, PSS, and FITC-PAH. Additional layers of PSS and PEI were deposited on top of the FITC-PAH layer to prevent rapid bleaching of the FITC due to oxidation by ambient air. The driving force for binding between PEI and gold is the interaction between the amine functionalities and gold.[32] Although the coverage of the Au_{NP} is below 100%,[13,18,33] we adsorbed the Au_{NP} on a single PEI layer (thickness of ca. 1 nm, as determined from QCM) to localize the nanoparticles on top of a thin layer. The washing solution was pure water, and the sample was dried after each washing step. For all adsorption solutions, except the Au_{NP} suspension, the adsorption time (t_a) was fixed at 20 min. The amount of Au_{NP} deposited was controlled by changing t_a for Au_{NP} deposition. The extinction spectra of the samples are shown in Figure 3b. The sample at $t_a = 0$ contains no Au_{NP}, and exhibits an FITC absorption peak at 507 nm (Figure 3b, spectrum 1). As t_a of the Au_{NP} suspension increases, the Au_{NP} SP band around 540 nm increases, reflecting an increase in the adsorbed amount of the nanoparticles. Higher Au_{NP} loadings result in a red shift and broadening of the SP band due to enhanced nanoparticle interactions, reflecting increased packing of the Au_{NP}.[34−36] The corresponding fluorescence spectra of these samples are shown in Figure 3c. The fluorescence peak of FITC was observed at 528 nm, and its intensity progressively decreased with increasing Au_{NP} amount. Figure 3d shows the normalized peak intensities at 528 nm of the spectra as a function of the extinction at 528 nm obtained from Figure 3b.

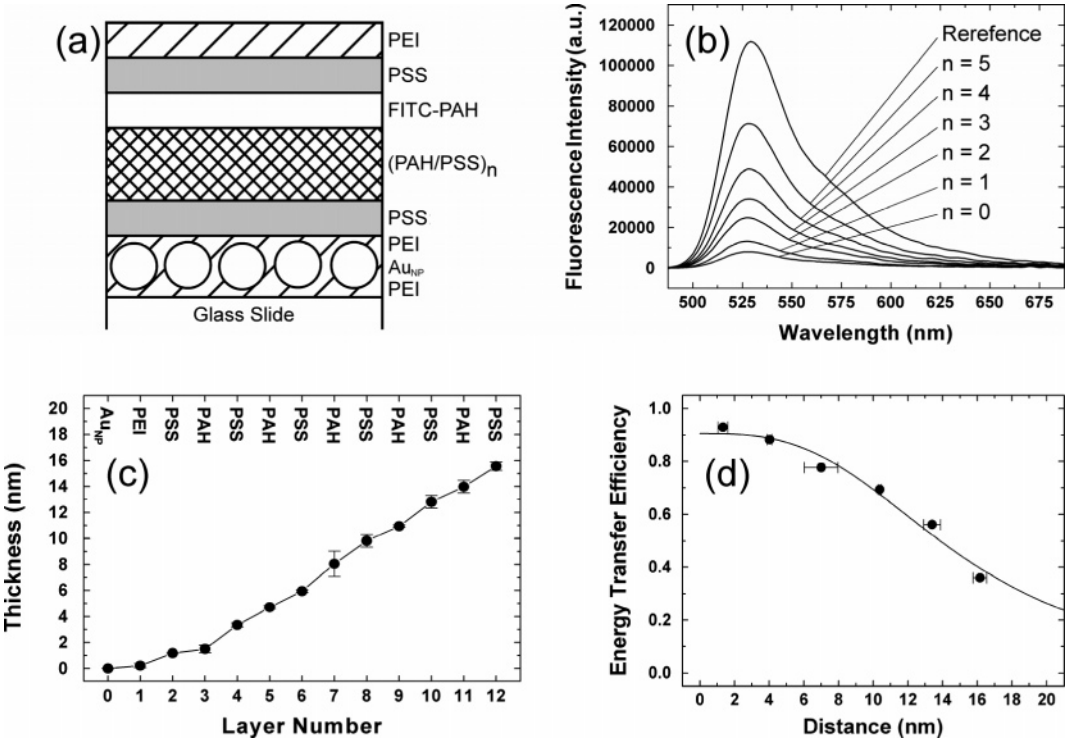

Figure 4. (a) Schematic of the cross section of the LbL film PEI/Au_{NP}/PEI/PSS/$(PAH/PSS)_n$/FITC-PAH/PSS/PEI, where n indicates the number of PAH/PSS bilayers. (b) Fluorescence spectra of the samples for $n = 0$, 1, 2, 3, 4, and 5, and the reference sample PEI//PSS/$(PAH/PSS)_2$/FITC-PAH/PSS/PEI that contains no Au_{NP}. (c) Thickness of the PAH/PSS film "spacer" between the Au_{NP} and FITC-PAH layers in the samples, as determined by QCM measurements, versus layer number. (d) Dependence of the ET efficiency on the distance determined in (c). The solid line represents the fitted curve using the equation of the effective ET efficiency $E_{eff} = \alpha E$ (see text for details).

As t_a increases, the normalized intensity approaches zero. However, the intensity plateaus at ca. 0.1 at $t_a = 20$ min (point 7), corresponding to 90% quenching of the fluorescence intensity of the sample at $t_a = 0$ (Figure 3d). The absence of complete quenching may be due to less than monolayer coverage of the Au_{NP} on the PEI film. It is noted that for 90% quenching of the FITC fluorescence, a 10-fold larger extinction of Au_{NP} than the absorption of FITC is required (Figure 3b).

The sample structure for experiment II is shown in Figure 4a. PAH/PSS bilayers were used to control the distance between the Au_{NP} and FITC-PAH layers. As for experiment I, the washing solution was pure water, and the sample was dried after each washing step. The t_a was fixed at 20 min for all PE adsorption solutions as well as the Au_{NP} suspension to maximize quenching, as determined from Figure 3c. The number of PAH/PSS bilayers, n, was altered from 0 to 5 (Figure 4a). A reference sample without Au_{NP} was prepared with an $n = 2$ layer structure, omitting the Au_{NP} deposition step and the subsequent PEI layer. The fluorescence spectra are shown in Figure 4b. As the distance between the Au_{NP} and the FITC-PAH layers increased, the fluorescence intensity increased. To determine the length of the spacing, QCM measurements were applied to a film with the same structure. The data are shown in Figure 4c. (The bottom two layers (PEI/Au_{NP}) and the top three layers (FITC-PAH/PSS/PEI) are omitted.) The increase in thickness calculated from the observed QCM frequency differences using eq 2 are plotted as a function of layer number. After three PE layers were deposited on the Au_{NP} layer, linear PE film growth was observed. The average thickness of the PSS/PAH bilayer was 2.7 nm, and the PSS and PAH layers were 1.5 and 1.2 nm, respectively. These thicknesses correspond well with those reported for the same polyelectrolytes deposited under similar conditions (0.5−1.5 nm).[31,37,38] Using the fluorescence intensity (I_∞) observed for the reference sample, the distance-dependent fluorescence intensity (I_d) shown in Figure 4b can be converted to an ET efficiency (quenching efficiency, E), using $E = 1 - I_d/I_\infty$.[39−41] The peak intensity at 528 nm was used for this calculation, and the plot of E as a function of distance is shown in Figure 4d. The distances were calculated from the top of the Au_{NP} layer to the center of the FITC-PAH layer (Figure 4c), assuming that FITC-PAH formed a layer with the same thickness as PAH. On the other hand, the E dependence on the distance between acceptor and donor d is written as[39,40]

$$E = \frac{1}{1 + (d/d_0)^x} \tag{3}$$

where d_0 is the critical distance of d at $E = 50\%$, and x depends on the dimensionality of the system.[42] In ideal cases, when a donor molecule transfers its energy to an acceptor molecule, $x = 6$ (Förster type).[39] For energy transfer to a two-dimensional array of acceptor molecules, $x = 4$,[43,44] and when a donor molecule transfers energy to a three-dimensional array of acceptor molecules (or a planar bulk metal film), $x = 3$.[45−47] To account for the quenching of less than 100%, observed in Figure 3d, a parameter α was introduced into eq 3. An effective ET efficiency $E_{eff} = \alpha E$ was used for fitting the data in Figure 4d. The best fit, shown as a solid line in Figure 4d, was obtained for $\alpha = 0.905$, $x = 3.0$, and $d_0 = 14.9$ nm. The value for α reflects the 90% quenching observed for sample $t_a = 20$ min, as shown in Figure 3c. The value for x implies that our samples correspond to a system where a donor molecule transfers its energy to a planar bulk metal film. This geometry is not appropriate for our samples shown in Figure 4a; i.e., the metal layer consists of Au_{NP} and not a bulk metal layer. In other work, the dependence of the emission yield of molecules as a function of distance was calculated where the molecule was near a single silver nanoparticle of 20 nm diameter or near a planar cluster

formed by five silver nanoparticles.[48] When the molecules oriented to the surface of the particle or the plane of the cluster, Liver et al. estimated x at ca. 2.5 and 3.5, respectively.[48] Therefore, the obtained x value (3.0) in our work reflects the superposition of the local ET from FITC to individual Au_{NP}, two-dimensional clusters of Au_{NP}, and three-dimensional clusters of Au_{NP} that give x as 2.5, 3.5, and 3, respectively. The obtained d_0 value (14.9 nm) in our system is much larger than the typical value in the Förster-type energy transfer (2−6 nm),[39] as a result of resonant ET.[46,48−50] It is well-known that PE layers in LbL assembled multilayers interpenetrate adjacent layers.[41,51] When the distribution function of the FITC-PAH layer along the film thickness was expressed by a Gaussian distribution function, the calculated α, x, and d_0 did not change significantly (less than 10%), even if the full width at half-maximum of the distribution function increased to 4 nm.

The features of the ET from FITC-PAH to Au_{NP} in the LbL films are summarized as follows. To obtain 90% quenching of the FITC fluorescence by the Au_{NP} located close to the fluorophore, the Au_{NP} extinction required is approximately 10 times larger than the FITC absorption (Figure 3b). The quenching efficiency exhibits a cubic dependence on the distance, with an apparent critical distance of 14.9 nm (Figure 4d). For a biosensor, it is expected that this large critical distance would contribute to the quenching of fluorophores that are conjugated to large proteins, e.g., immunoglobulin G, with a size of about 10 nm,[52,53] making the current system attractive for such studies.

(b) Binding Properties of B-PAH. NMR experiments reveal a biotin labeling of 4% of the monomer units in the polymer. However, the activity of biotin on B-PAH and the evidence of a *covalent bond* between biotin and the polymer backbone cannot be observed by NMR measurements. Therefore, two experiments were performed before constructing the sensor. First, the binding activity of B-PAH against avidin was investigated by HABA assay. The solution of PAH of M_w = 15 000 did not induce any change in the absorption spectrum of the avidin−HABA complex in solution. However, the B-PAH solution clearly induced a change in the spectrum, namely a decrease in the absorption of the avidin−HABA complex at 500 nm. This result confirms B-PAH has biotin molecules that are accessible to avidin. The aging effect on the B-PAH solution was also investigated by HABA assay. After refrigeration for 1 month, a 20% decrease of the affinity was observed.

Further evidence that the PAH was biotinylated was provided by constructing a LbL film from B-PAH and FITC-avidin.[22,54] B-PAH is positively charged because of the allylamine groups. Also, the net surface charge of avidin at pH 7.3 is positive, as it has an isoelectric point of 10.[55] Therefore, a B-PAH/avidin multilayer should not form through electrostatic interactions. A multilayer can, however, be built through specific binding between the biotin of B-PAH and avidin, if biotin molecules are covalently attached to the polymer chain. B-PAH/FITC-avidin multilayers were assembled on a PEI/$(PSS/PAH)_2$/PSS precursor film by the sequential deposition of B-PAH (0.25 mg mL^{-1} in HEPES) and FITC-avidin (1.6 mg mL^{-1} in HEPES). An adsorption time of 10 min was used for both solutions. HEPES buffer was used as the washing solution, and the films were not dried during the coating and the fluorescence measurements to prevent avidin denaturation.[56] As a control, PAH was used under the same conditions to prepare a PAH/FITC-avidin multilayer film. The layer growth was monitored by fluorescence measurements. Despite the adsorption of FITC-avidin on the first PAH layer, regular film growth was only observed for the B-PAH/FITC-avidin film (Figure 5). The unspecific binding of

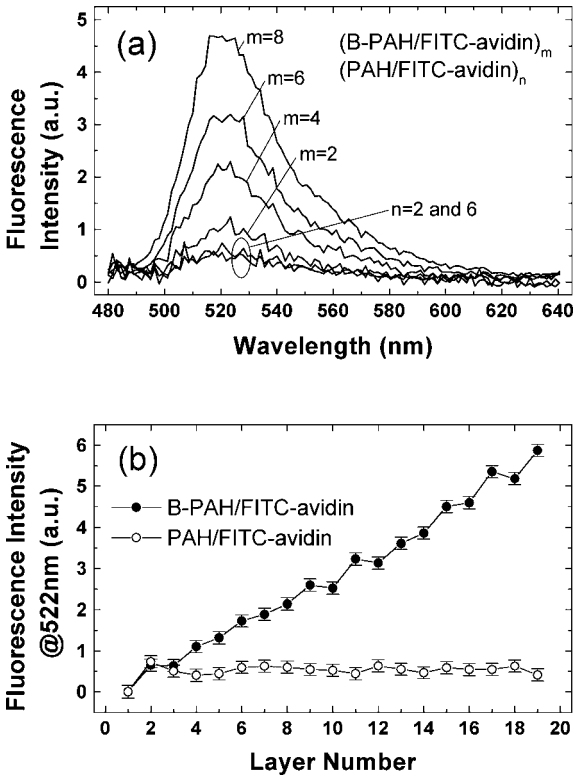

Figure 5. (a) Fluorescence spectra for the formation of B-PAH/FITC-avidin and PAH/FITC-avidin films. (b) Fluorescence intensity at 522 nm for the films as a function of layer number. The odd and even numbers indicate B-PAH (or PAH) and FITC-avidin layers, respectively.

FITC-avidin on the first layer of PAH could be due to the electrostatic interaction between FITC-avidin and the negatively charged PSS layer beneath the first PAH layer. The above experiments and the 4% labeling of the monomer units, determined from NMR, provide strong evidence that the prepared B-PAH has covalently bound biotin molecules, which exhibit a high binding activity to avidin.

Microspheres. *(a) LbL Coating of PS Latexes.* To increase the loading of Au_{NP} on the latexes so as to ensure maximum quenching of the immobilized FITC-anti-biotin IgG, three PAH/PSS bilayers were deposited as a precursor film (rather than a single PEI layer). We have shown that the Au_{NP} distribution through such a film is homogeneous and dense.[13,18,33] After three bilayers of PAH/PSS were coated on the bare latexes of 488 nm diameter, Au_{NP} were adsorbed by exposing the $(PAH/PSS)_3$-coated latexes to the Au_{NP} dispersion for 12 h. The TEM images of the PS latexes coated with $(PAH/PSS)_3/Au_{NP}$ are shown in Figure 6a,b. Uniformly sized spheres with a dense Au_{NP} coating were observed, as previously reported.[13,18,33] Two PEI/PSS bilayers were deposited following the Au_{NP} adsorption step. TEM images of the PS latexes coated with $(PAH/PSS)_3/Au_{NP}/(PEI/PSS)_2$/B-PAH are shown in Figure 6c,d. No significant desorption of Au_{NP} was observed upon the subsequent deposition of $(PEI/PSS)_2$/B-PAH.

For the competitive assay for biotin, FITC-anti-biotin IgG was bound to biotinylated Au_{NP}/PE latexes (PS latex/$(PAH/PSS)_3/Au_{NP}/(PEI/PSS)_2$/B-PAH). The anti-biotin IgG has a lower binding constant to biotin (10^6−10^9 M^{-1}) than avidin (10^{15} M^{-1}),[57] indicating that anti-biotin IgG is more suitable than avidin for a competitive-binding assay for biotin. The TEM images of the FITC-anti-biotin IgG bound biotin−Au_{NP}/PE latexes are shown in Figure 6e,f. Again, there was no evidence for desorption of the Au_{NP}. The pronounced gray layer at the

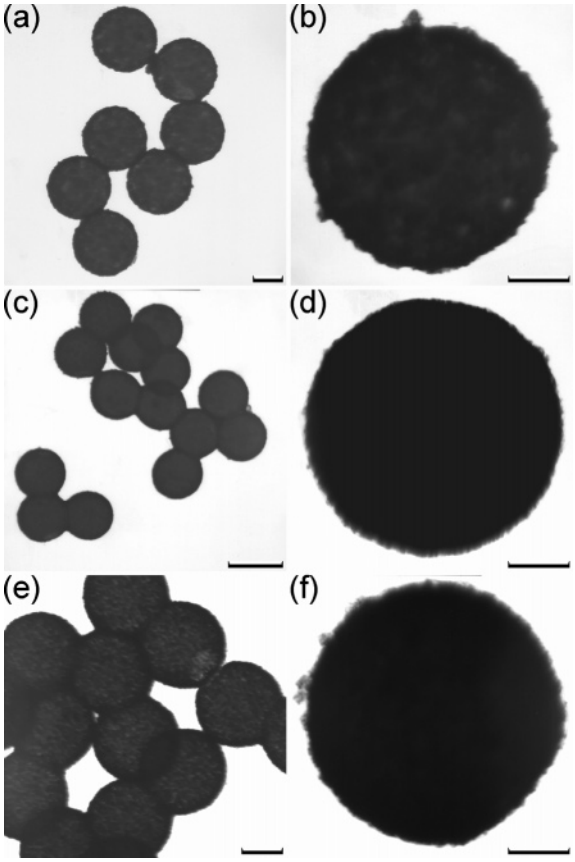

Figure 6. TEM images of the coated PS latexes. (a, b) PS latex/(PAH/PSS)$_3$/Au$_{NP}$. Scale bars are 220 (a) and 120 nm (b). (c, d) PS latex/(PAH/PSS)$_3$/Au$_{NP}$/(PEI/PSS)$_2$/B-PAH. Scale bars are 520 (c) and 120 nm (d). (e, f) PS latex/(PAH/PSS)$_3$/Au$_{NP}$/(PEI/PSS)$_2$/B-PAH/FITC-anti-biotin IgG. Scale bars are 240 (e) and 120 nm (f). When the suspension consisted of the buffer solution, the suspension was washed with pure water to remove salts and avoid salt crystals appearing in the TEM images.

edge of the latex in Figure 6f indicates a thick layer of organic material, such as PE, FITC-anti-biotin IgG, and BSA (which was present in the buffer). The suspensions of the coated latexes displayed good colloidal stability.

Our previous work has shown that the film thickness on particles and planar surfaces is similar for PAH/PSS multilayers.[38] Therefore, the same film deposited on the particles was assembled on the QCM electrodes to determine the PE layer thicknesses for the film assembled on the latexes (Figure 7a). The same deposition conditions were employed as for the particle coating, with the exception of a drying step used after adsorption of each layer on the QCM. The measured frequency differences were converted to layer thicknesses using eq 2. The QCM measurements suggest that the Au$_{NP}$ layer on the latexes corresponds to a 14.6 nm thick gold layer. The QCM data also show linear film growth for the PAH/PSS and PEI/PSS layers (Figure 7a).

The amount of biotin on the latex particles was evaluated from complementary QCM measurements on the same films. A B-PAH layer thickness of 2.6 nm (Figure 7a) corresponds to $\Delta f = -154$ Hz. The surface area of a single coated latex particle (PS latex/(PAH/PSS)$_3$/Au$_{NP}$/(PEI/PSS)$_2$) is calculated as 0.95 μm^2, taking into account the increase in diameter from 488 to 550 nm due to the PE and the Au$_{NP}$ layers, and considering the coated particles as smooth spheres. Therefore, using eq 1, the total mass of the B-PAH adsorbed per latex particle equals 4×10^{-15} g. Using the 4% biotin labeling of PAH, the number of

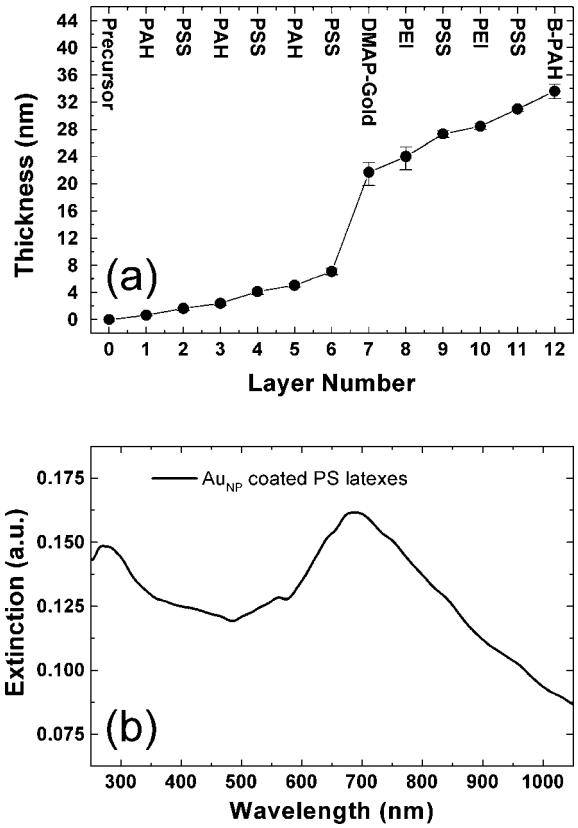

Figure 7. (a) QCM layer thicknesses for a (PAH/PSS)$_3$/Au$_{NP}$/(PEI/PSS)$_2$/B-PAH film on the PEI/PSS precursor. Data represent the average of four independent samples. (b) Extinction spectrum of the suspension of the PS latexes coated with (PAH/PSS)$_3$/Au$_{NP}$/(PEI/PSS)$_2$/B-PAH.

biotin molecules per latex is calculated as 9.1×10^5, corresponding to a surface coverage of approximately 1 biotin molecule per nm^2.

The extinction spectrum of the suspension in Figure 7b shows a plasmon peak at 685 nm. The further red shift and broadening of the plasmon band, compared to that in Figure 3b, implies a denser packing of Au$_{NP}$ on the PS latexes, which promotes coupling of the SP modes of adjacent Au$_{NP}$.[13,18,33−36] Although a further red shift causes an off-resonant ET from FITC to the Au$_{NP}$ SP mode, the broadening of the plasmon band sustains the ET close to the resonant state. There is still an overlap between the plasmon band at 685 nm, which has a tail down to 500 nm, and the fluorescence band of FITC around 520 nm, which tails up to 650 nm.

(b) Competitive FQIA Using LbL Coated PS Latexes. The fluorescence spectrum of the suspension before starting the titration showed a slanted line with higher intensity at shorter wavelengths, indicating stray light from the excitation beam, which is attributed to scattering from the coated latexes. However, the contribution of the fluorescence from FITC on the IgG having a typical size of 10 nm[52,53] was not visible, suggesting that the characteristic long critical distance d_0 similar to that observed in the planar films (Figure 4b) was realized on the latexes. This spectrum of the stray light was adopted as a background for each fluorescence spectrum. Fluorescence spectra at certain cumulative amounts of the titrated biotin are shown in Figure 8a. The spectra indicate an increase and saturation of the fluorescence intensity. Such responses were reproducible using different batches of coated latexes. Figure 8b shows the titration curve of the fluorescence intensity at 522 nm as a function of the total biotin amount. A steep increase in fluorescence intensity was observed until 50 nmol of biotin,

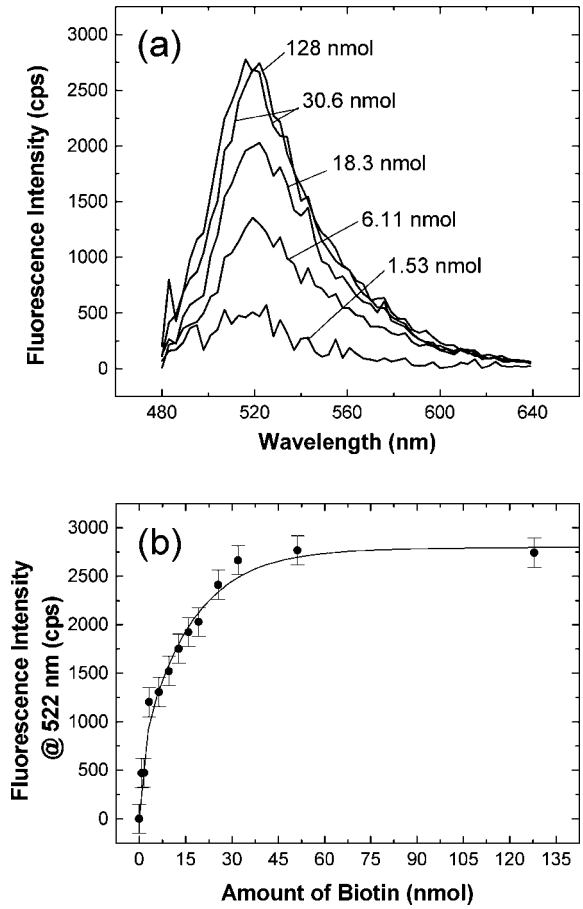

Figure 8. (a) Fluorescence spectra for the PS latexes coated with (PAH/PSS)$_3$/Au_{NP}/(PEI/PSS)$_2$/B-PAH/FITC-anti-biotin IgG after titration with biotin solution. The amount indicated for each spectrum is the cumulative amount of biotin added. (b) Titration curve of the fluorescence intensity at 522 nm. The transverse axis shows the cumulative amount of biotin added. The solid line is drawn to guide the eye.

and above this concentration, the intensity saturated. Therefore, the dynamic range of this sensor is from 1 to 50 nmol (total number of particles = 10^{11}). By accounting for the saturation of the response at 50 nmol of biotin, one latex particle is responsible for 2.9×10^5 biotin molecules, representing one-third of the number of the fixed biotin molecules on the latex (9.1×10^5; see the section LbL Coating of PS Latexes). Having fewer reacted free biotin molecules than immobilized biotins on the latex is quite reasonable, because FITC-anti-biotin IgG has a larger molecular size and could bind with a lower density than the biotin immobilized on the latex. The negative control experiment was performed using the Au_{NP}/PE latexes, which had PAH instead of B-PAH. These particles were incubated with FITC-anti-biotin IgG, and no increase of fluorescence intensity was observed upon the addition of biotin solution. These results demonstrate the successful application of Au_{NP}/PE-coated submicron-size latexes tailored by the LbL technique in homogeneous and competitive FQIAs.

Conclusions

The resonant ET from FITC to the SP band of Au_{NP} was investigated by changing the distance between the Au_{NP} and FITC-PAH layers in LbL assembled thin films on planar supports. The quenching efficiency depends on the cube of the distance, and the apparent critical distance (50% quenching efficiency) was ca. 15 nm, which is more than twice the typical value observed for Förster-type ET, as a result of the resonant ET to the SP modes of Au_{NP}. B-PAH was synthesized to form a biosensor, and its high specificity for avidin binding allowed the preparation of B-PAH/avidin LbL multilayers. Au_{NP}/PE films, which were assembled on colloidal particles and after modification with B-PAH and FITC-anti-biotin IgG, were employed in a homogeneous and competitive FQIA for biotin. The characteristic long critical distance of the resonant ET was utilized to quench FITC conjugated to the IgG (size ~10 nm). The particles exhibited a dynamic range of 1−50 nmol for analyte (biotin) detection. The demonstrated techniques for surface tailoring of submicron-sized latexes, based on the LbL method, could be used to develop particle-based optical biosensors, with tunable dynamic sensing ranges.

Acknowledgment. This work was supported by the Australian Research Council under the Federation Fellowship and Discovery Project Schemes. N.K. acknowledges the JSPS for a Research Fellowship for Young Scientists.

References and Notes

(1) Wood, P. J.; Barnard, G. In *Principles and Practice of Immunoassay*, 2nd ed.; Price, C. P., Newman, D. J., Eds.; Stockton Press: New York, 1997; Chapter 16, pp 389−424.
(2) Hage, D. S. *Anal. Chem.* **1999**, *71*, 294R.
(3) (a) Wolfbeis, O. S. *Anal. Chem.* **2000**, *72*, 81R. (b) Kürner, J. M.; Wolfbeis, O. S.; Klimant, I. *Anal. Chem.* **2002**, *74*, 2151.
(4) Dubertret, B.; Calame, M.; Libchaber, A. *Nat. Biotechnol.* **2001**, *19*, 365.
(5) Maxwell, D. J.; Taylor, J. R.; Nie, S. *J. Am. Chem. Soc.* **2002**, *124*, 9606.
(6) Barker, S. L. R.; Kopelman, R. *Anal. Chem.* **1998**, *70*, 4902.
(7) Franz, K. J.; Singh, N.; Spingler, B.; Lippard, S. J. *Inorg. Chem.* **2000**, *39*, 4081.
(8) Wang, G.; Zhang, J.; Murray, R. W. *Anal. Chem.* **2002**, *74*, 4320.
(9) Shepherd, J. L.; Kell, A.; Chung, E.; Sinclar, C. W.; Workentin, M. S.; Bizzotto, D. *J. Am. Chem. Soc.* **2004**, *126*, 8329.
(10) Pèrez-Luna, V. H.; Yang, S.; Rabinovich, E. M.; Buranda, T.; Sklar, L. A.; Hampton, P. D.; López, G. P. *Biosens. Bioelectron.* **2002**, *17*, 71.
(11) Lakowicz, J. R.; Shen, Y.; D'Auria, S.; Malicka, J.; Fang, J.; Gryczynski, Z.; Gryczynski, I. *Anal. Biochem.* **2002**, *301*, 261.
(12) Lakowicz, J. R.; Malcka, J.; Gryczynski, I.; Gryczynski, Z.; Geddes, C. D. *J. Phys. D: Appl. Phys.* **2003**, *36*, R240.
(13) Liang, Z.; Susha, A. S.; Caruso, F. *Adv. Mater.* **2002**, *14*, 1160.
(14) Liang, Z.; Susha, A.; Caruso, F. *Chem. Mater.* **2003**, *15*, 3176.
(15) Miclea, P. T.; Susha, A. S.; Liang, Z.; Caruso, F.; Sotomayor Torres, C. M.; Romanov, S. G. *Appl. Phys. Lett.* **2004**, *84*, 3960.
(16) Radt, B.; Smith, T. A.; Caruso, F. *Adv. Mater.* **2004**, *16*, 2184.
(17) Angelatos, A. S.; Radt, B.; Caruso, F. *J. Phys. Chem. B* **2005**, *109*, 3071.
(18) Gittins, D. I.; Susha, A. S.; Schoeler, B.; Caruso, F. *Adv. Mater.* **2002**, *14*, 508.
(19) Gittins, D. I.; Caruso, F. *Angew. Chem., Int. Ed.* **2001**, *40*, 3001.
(20) Hermanson, G. T. *Bioconjugate Techniques*; Academic Press: London, 1996; Chapter 8, pp 303−305.
(21) Yang, W.; Trau, D.; Renneberg, R.; Yu, N. T.; Caruso, F. *J. Colloid Interface Sci.* **2001**, *234*, 356.
(22) Anzai, J.; Kobayashi, Y.; Nakamura, N.; Nishimura, M.; Hoshi, T. *Langmuir* **1999**, *15*, 221.
(23) Lindegren, S.; Andersson, H.; Jacobsson, L.; Bäck, T.; Skarnemark, G.; Karlsson, B. *Bioconjugate Chem.* **2002**, *13*, 502.
(24) Reddy, D. V.; Shenoy, B. C.; Carey, P. R.; Sönnichsen, F. D. *Biochemistry* **1997**, *36*, 14676.
(25) Salem, A. K.; Cannizzaro, S. M.; Davies, M. C.; Tendler, S. J. B.; Roberts, C. J.; Williams, P. M.; Shakesheff, K. M. *Biomacromolecules* **2001**, *2*, 575.
(26) Schoeler, B.; Kumaraswamy, G.; Caruso, F. *Macromolecules* **2002**, *35*, 889.
(27) Green, N. M. *Biochem. J.* **1965**, *94*, 23c.
(28) Livnah, O.; Bayer, E. A.; Wilchek, M.; Sussman, J. L. *FEBS Lett.* **1993**, *328*, 165.
(29) Sauerbrey, G. *Z. Phys.* **1959**, *155*, 206.
(30) Lvov, Y.; Ariga, K.; Ichinose, I.; Kunitake, T. *J. Am. Chem. Soc.* **1995**, *117*, 6117.
(31) Caruso, F.; Niikura, K.; Furlong, D. N.; Okahata, Y. *Langmuir* **1997**, *13*, 3422.

(32) (a) Leff, D. V.; Brandt, L.; Heath, J. R. *Langmuir* **1996**, *12*, 4723. (b) Chen, X. Y.; Li, J. R.; Jiang, L. *Nanotechnology* **2000**, *11*, 108. (c) Brown, L. O.; Hutchison, J. E. *J. Am. Chem. Soc.* **1999**, *121*, 882. (d) Mukhopadhyay, K.; Phadtare, S.; Vinod, V. P.; Kumar, A.; Rao, M.; Chaudhari, R. V.; Sastry, M. *Langmuir* **2003**, *19*, 3858. (e) Selvakannan, P. R.; Mandal, S.; Pasricha, R.; Adyantaya, S. D.; Sastry, M. *Chem. Commun.* **2002**, 1334.

(33) Cho, J.; Caruso, F. *Chem. Mater.* **2005**, *17*, 4547.

(34) Mayya, K. S.; Schoeler, B.; Caruso, F. *Adv. Funct. Mater.* **2003**, *13*, 183.

(35) Schmitt, J.; Mächtle, P.; Eck, D.; Möhwald, H.; Helm, C. A. *Langmuir* **1999**, *15*, 3256.

(36) (a) Corbierre, M. K.; Cameron, N. S.; Sutton, M.; Mochrie, S. G. J.; Lurio, L. B.; Rühm, A.; Lennox, R. B. *J. Am. Chem. Soc.* **2001**, *123*, 10411. (b) Malikova, N.; Pastoriza-Santos, I.; Schierhorn, M.; Kotov, N. A.; Liz-Marzán, L. M. *Langmuir* **2002**, *18*, 3694. (c) Jiang, C.; Markutsya, S.; Tsukruk, V. V. *Langmuir* **2004**, *20*, 882.

(37) Decher, G.; Schmitt, J. *Prog. Colloid Polym. Sci.* **1992**, *89*, 160.

(38) Caruso, F.; Lichtenfeld, H.; Donath, E.; Möhwald, H. *Macromolecules* **1999**, *32*, 2317.

(39) Wu, P.; Brand, L. *Anal. Biochem.* **1994**, *218*, 1.

(40) Chirio-Lebrun, M.-C.; Parts, M. *Biochem. Educ.* **1998**, *26*, 320.

(41) Baur, J. W.; Rubner, M.; Reynolds, J. R.; Kim, S. *Langmuir* **1999**, *15*, 6460.

(42) Waldeck, D. H.; Alivisatos, A. P.; Harris, C. B. *Surf. Sci.* **1985**, *158*, 103.

(43) Bücher, H.; Drexhage, K. H.; Fleck, M.; Kuhn, H.; Möbius, D.; Schäfer, F.-P.; Sondermann, J.; Sperling, W.; Tillmann, P.; Wiegand, J. *Mol. Cryst.* **1967**, *2*, 199.

(44) Kuhn, H.; Möbius, D. *Angew. Chem., Int. Ed. Engl.* **1971**, *10*, 620.

(45) Haynes, D. R.; Tokmakoff, A.; George, S. M. *J. Chem. Phys.* **1994**, *100*, 1968.

(46) Chance, R. R.; Prock, A.; Silbey, R. In *Advances in Chemical Physics*; Prigogine, I., Rice, S. A., Eds.; John Wiley & Sons: New York, 1978; Vol. 37, pp 1−65.

(47) Kurczewska, H.; Bässler, H. *J. Lumin.* **1977**, *15*, 261.

(48) Liver, N.; Nitzan, A.; Freed, K. F. *J. Chem. Phys.* **1985**, *82*, 3831.

(49) Ruppin, R. *J. Chem. Phys.* **1982**, *76*, 1681.

(50) Pineda, A. C.; Ronis, D. *J. Chem. Phys.* **1985**, *83*, 5330.

(51) Decher, G. *Science* **1997**, *277*, 1232.

(52) Root, D. D. *Proc. Natl. Acad. Sci. U.S.A.* **1997**, *94*, 5685.

(53) Hastings, R. H.; Grady, M.; Sakuma, T.; Matthay, M. A. *J. Appl. Physiol.* **1992**, *73*, 1310.

(54) Cassier, T.; Lowack, K.; Decher, G. *Supramol. Sci.* **1998**, *5*, 309.

(55) Green, N. M. *Adv. Protein Chem.* **1975**, *29*, 85.

(56) Caruso, F.; Rodda, E.; Furlong, N.; Niikura, K.; Okahata, Y. *Anal. Chem.* **1997**, *69*, 2043.

(57) Kilpatrick, P. K.; Lisi, J. F.; Carbonell, R. G. *Biotechnol. Prog.* **1997**, *13*, 446.